

Article

Solid Bitumen Occurrences in the Pyrenean Basin (Southern France): A Case Study across the Pliensbachian–Toarcian Boundary

Carolina Fonseca ^{1,*}, João Graciano Mendonça Filho ², Carine Lézin ¹, Frederico Sobrinho da Silva ² and Luís V. Duarte ³

¹ Géosciences Environnement Toulouse, University of Toulouse, CNES, CNRS, IRD, UPS, 31400 Toulouse, France; carine.lezin@get.omp.eu

² Laboratório de Palinofácies e Fácies Orgânica (LAFO), Departamento de Geologia, Instituto de Geociências, Federal University of Rio de Janeiro, Rio de Janeiro 21941-916, Brazil; graciano@geologia.ufrj.br (J.G.M.F.); fsobrinho@lafo.geologia.ufrj.br (F.S.d.S.)

³ MARE-Marine and Environmental Sciences Centre, Department of Earth Sciences, Faculty of Sciences and Technology, University of Coimbra, 3030-790 Coimbra, Portugal; lduarte@dct.uc.pt

* Correspondence: cmfonseca13@gmail.com

Abstract: The study across the Pliensbachian–Toarcian boundary sedimentary record in the Bizanet section of the Pyrenean Basin (southern France) revealed the presence of solid bitumen. This secondary organic matter was characterized using petrographic (transmitted and reflected white lights, incident blue light, and scanning electron microscopy) and geochemical (total organic carbon, total sulfur, and insoluble residue) techniques. The spore coloration index (SCI) was also determined. With the characterization of the optical properties and reflectance of the solid bitumen, it was possible to distinguish four different families (A–D) that display a wide range of reflectance values, from 0.21% to 2.64% BR_r, i.e., from glance pitch to meso-impsonite. SCI values were higher than 9–9.5 (%R_{eq} > 1.50%). The comparison between the equivalent vitrinite reflectance values of the solid bitumen and SCI showed that this index and the solid bitumen D values are concordant, indicating that solid bitumen D can be considered an indigenous bitumen. The other three families of solid bitumen (A–C) are considered as having migrated. The laterally equivalent Pont de Suert section (South Pyrenean Zone) displays no trace of solid bitumen which points to the important role of the morphotectonic context of the Bizanet section in the migration of these hydrocarbons, namely, the presence of a major thrust fault in the eastern Corbières close to the section's location.

Keywords: solid bitumen; thermal maturity; solid bitumen reflectance; spore coloration index; Pliensbachian–Toarcian; Pyrenean Basin



check for updates

Citation: Fonseca, C.; Mendonça Filho, J.G.; Lézin, C.; Sobrinho da Silva, F.; Duarte, L.V. Solid Bitumen Occurrences in the Pyrenean Basin (Southern France): A Case Study across the Pliensbachian–Toarcian Boundary. *Minerals* **2021**, *11*, 1338. <https://doi.org/10.3390/min11121338>

Academic Editor: Leszek Marynowski

Received: 20 October 2021

Accepted: 25 November 2021

Published: 29 November 2021

Publisher's Note: MDPI stays neutral with regard to jurisdictional claims in published maps and institutional affiliations.



Copyright: © 2021 by the authors. Licensee MDPI, Basel, Switzerland. This article is an open access article distributed under the terms and conditions of the Creative Commons Attribution (CC BY) license (<https://creativecommons.org/licenses/by/4.0/>).

1. Introduction

In source-rock reservoirs, it is possible to find two types of organic matter (OM): primary and secondary. Primary OM is the one that is originally from the depositional setting (kerogen and original soluble OM, i.e., not a product of generation/expulsion), while secondary OM has its origin in the transformation of primary OM e.g., [1–6]. Secondary OM is divided by organic geochemists into extractable and non-extractable materials, the so-called bitumen and pyrobitumen, respectively. In organic petrology, international nomenclature classifies oil, solid bitumen, and pyrobitumen as secondary OM. These components are usually dominant in sedimentary sequences with maturities in the late oil and dry gas windows. This heavily influences the reservoir quality as certain types of solid bitumen behave as a cement, reducing reservoir porosity and permeability e.g., [6–12]. Furthermore, solid bitumen reflectance can be used to assess maturity in the absence of vitrinite and also provide information on the migration pathway e.g., [13–15].

In organic petrology, solid bitumen corresponds to solid OM that can be found filling voids and fractures in sedimentary rocks (both carbonates and siliciclastic) that result from thermal maturation [14,16]. Based on their physical properties (e.g., reflectance, fluorescence intensity, micro-solubility), Jacob [14] proposed their classification into ozocerite, wurtzilite, albertite, asphalt, gilsonite, glance pitch, grahamite, and impsonite (epi-, meso-, and cata-impsonite).

In organic chemistry, bitumen is classified as the OM soluble in organic solvents. It is possible to classify bitumen with regard to oil generation into pre-oil bitumen and post-oil bitumen (or pyrobitumen) [16]. Pre-oil bitumen is an early-generation product (viscous fluid) that migrated a minimum distance before reaching the fractures and voids in the rock. Post-oil bitumen is an alteration product of crude oil that is generated and migrated from a source rock [16].

Many studies focus their attention on the characterization of solid bitumen using both petrographic and geochemical approaches to try to define its origin and assess the thermal maturity of the sequences [7,13–30]. Recent reviews of solid bitumen characterization (e.g., origin, classification of physical and chemical properties), especially the one associated with source-rock reservoirs, and its implications for reservoir quality, porosity, permeability, and producibility were published by Mastalerz et al. [6] and Sanei [31].

For the Lower Jurassic sediments of the Pyrenean Basin, no occurrences of solid bitumen have been described, although an organic petrographic study of an upper Pliensbachian–lower Toarcian succession from the South Pyrenean Zone with special focus on thermal maturity assessment based on hydroid reflectance and SCI was published by Fonseca et al. [32]. With these premises, the main objectives of this study are as follows: (i) to characterize the solid bitumen identified in the upper Pliensbachian–lower Toarcian Bizanet section (eastern Pyrenees); (ii) to compare the solid bitumen reflectance to the spore coloration index values; and (iii) to discuss the relationship between the morphotectonic context of the Bizanet section and the solid bitumen occurrences.

2. Geological Setting

During the Triassic to Jurassic times, in the current-day Pyrenees, the displacement of the Pangea led to the creation of a subsiding Pyrenean Basin (PB). This basin extended between the Iberian and European tectonic plates and was controlled by Hercynian structures [33,34]. The Pyrenean tectonics that occurred between the latest Cretaceous and the Oligocene deformed, detached, and fragmented the substrate, resulting in diverse tectonic units [33,34]. The Bizanet section under study is located in the eastern Corbières and represents one of the reference sections of the eastern Pyrenees (Figure 1) [33]. The Corbières nappe covers the entire surface of the eastern Corbières, corresponding to the extension of the structural elements of the North Pyrenean Zone that suffered significant detachment. The tangential displacement of the Corbières nappe to NW and W–NW (about 20 km) favored by the Triassic evaporitic sediments occurred during the upper Eocene and is especially significant in the Fontjoncouse, Taura, and Bizanet areas. In terms of sedimentation, it is mostly characterized by Jurassic and Lower Cretaceous units [35].

The Bizanet section is characterized by an approximately 4 m thick succession of upper Pliensbachian–lower Toarcian sediments. The base of the outcrop is characterized by the limestone-dominated Barre a Pecten Formation (Fm.) (upper Pliensbachian), presenting two beds of bioclastic limestones rich in crinoids and bivalve fragments. These beds are topped by a sediment gap dated from the *Tenuicostatum* biozone. This sedimentary gap generated, in part, by erosion, as evidenced by the presence of an erosion surface, is followed by iron-bearing black marls and a bed of limestone with ferruginous oolites, a succession that is topped by a bed of dolomitic limestone dated from the *Serpentinum* biozone, *Elegantulum* subzone. This succession comprises the Schistes carton Member (Mb.) of the Bizanet Fm. This is followed by the Argilites noires litées Mb. of the Bizanet Fm. that is dominated by black marls dated from the *Bifrons* biozone (Figure 2) [33].

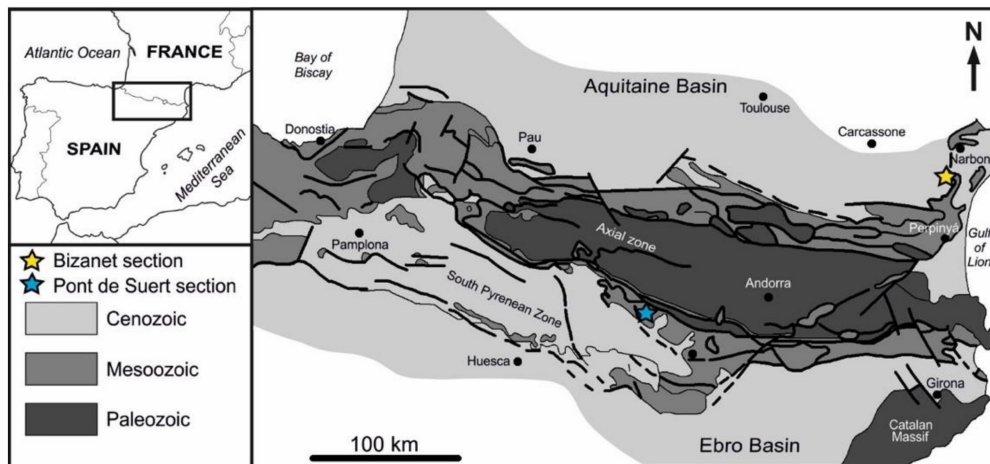


Figure 1. Simplified geological map of the Pyrenean Basin and location of the studied Bizanet section (adapted with permission from ref. [32]. Copyright 2018 Elsevier).

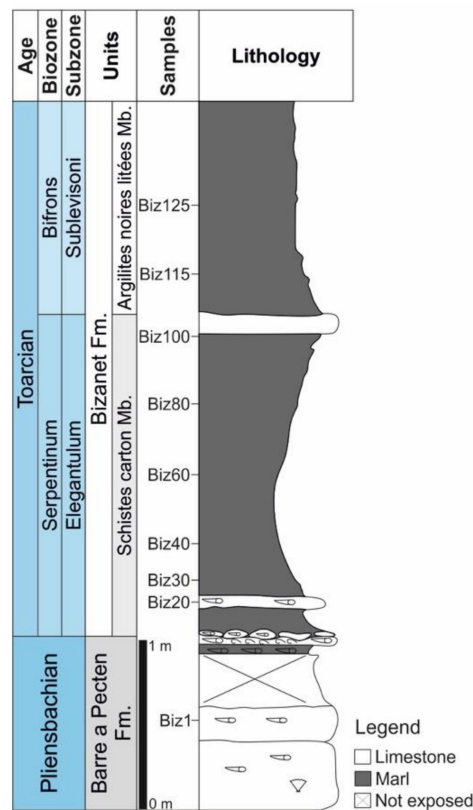


Figure 2. Stratigraphic log of the Bizanet section with sample location.

3. Materials and Methods

3.1. Materials

A set of nine samples belonging to the upper Pliensbachian–lower Toarcian succession of the Bizanet section was analyzed: one from the Barre a Pecten Fm., six from the Schistes carton Mb. of the Bizanet Fm., and two from the Argilites noires litées Mb. of the Bizanet Fm. The samples were collected at the Bizanet outcrop, and proper attention was given to the collection of fresh and unaltered samples.

3.2. Geochemical Analysis

Total organic carbon (TOC) and total sulfur (TS) contents were determined at the Laboratory of Palynofacies and Organic Facies of the Federal University of Rio de Janeiro (LAFO-UFRJ), Brazil, using a LECO SC 144 analyzer (LECO Corporation, St. Joseph, MI, USA) following the ASTM D4239-08 and NCEAC-C-1282 [36,37] standards. Insoluble residue (IR) corresponds to the fraction of sample not eliminated by acid treatment, presuming all the carbonates were eliminated.

3.3. Organic Matter Isolation

Isolated OM slides were prepared at LAFO-UFRJ following standard nonoxidative procedures according to Mendonça Filho et al. and Tyson [38–40] for isolation of the organic fraction from the rock matrix. This material was used for the identification of solid bitumen and determination of the spore coloration index using petrographic techniques (transmitted white and incident blue lights).

3.4. Spore Coloration Index (SCI)

This analysis was performed through the optical comparison of sporomorph coloration in transmitted white light with the LAFO-UFRJ standard slides with a scale of 1–10 and intervals of 0.5 using a Carl Zeiss Axio Imager A1 microscope (ZEISS, Oberkochen, Germany) with 20× magnification. The SCI, temperature, and age correlation chart proposed by Fisher et al. [41] was used for the determination of the equivalent vitrinite reflectance (VR_{eq}) values.

3.5. Scanning Electron Microscopy (SEM)

SEM analysis was performed in the isolated kerogen of one selected sample (Biz100). A drop of the isolated kerogen was deposited on a carbon ribbon, on an aluminum stub, and left to dry for 24 h. The observation of the nonmetallized sample was executed using a Zeiss EVO M10 Scanning Electron Microscope at LAFO-UFRJ with a 15.75 kV voltage (EHT) and a working distance (WD) of 8.5 mm under vacuum.

3.6. Organic Petrographic Analyses

Optical petrography was performed on whole-rock polished blocks prepared according to the standard procedures [42], and reflected white and incident blue lights were used to characterize the solid bitumen. The analyses were carried out at the Laboratory of Organic Petrography of the Institute of Earth Sciences (ICT) (Porto, Portugal) and the Department of Geosciences, Environment, and Spatial Planning of the Faculty of Sciences of the University of Porto (DGAOT-FCUP) (Porto, Portugal). The mean random reflectance was measured with a Leica DM4000 microscope equipped with a Discus-Fossil system using 50× magnification in immersion oil ($n_D = 1.518$ –23 °C) according to the ASTM D7708 [43] standard. Identification of the organic particles was based on their morphology and optical properties as proposed and described by Jacob [14], and their reflectance values were calculated to the equivalent of vitrinite reflectance using Equation (1) as proposed by Jacob [14]:

$$VR_{eq} = 0.618 \times BR_r + 0.4 \quad (1)$$

where VR_{eq} is the equivalent vitrinite reflectance and BR_r is the measured solid bitumen random reflectance.

4. Results and Discussion

4.1. Geochemistry

The TOC content varies between 0.25 and 2.03 wt.%, with the highest average value registered in the Schistes carton Mb. (1.31 wt.%). IR values vary between 12 and 82 wt.%, with the highest average value observed in the Schistes carton Mb. (51 wt.%). The lowest TOC and IR values are observed at the base of the section, in the Barre a Pecten Fm.

(0.31 and 12 wt.%, respectively). The total sulfur values are low throughout the section, ranging between 0.02 and 0.04 wt.% (Table 1).

Table 1. Geochemical data from the Bizanet section.

Sample	Lithology	Geochemistry		
		TOC (wt.%) ¹	Sulfur (wt.%) ²	IR (wt.%)
<i>Argilites noires litées Mb.</i>				
Biz125	Marl	1.28	0.03	50
Biz115	Calcareous marl	1.17	0.02	36
<i>Schistes carton Mb.</i>				
Biz100	Marly limestone	0.89	0.02	29
Biz80	Marl	2.03	0.04	47
Biz60	Marl	1.44	0.03	55
Biz40	Marl	1.79	0.04	82
Biz30	Marl	1.45	0.04	80
Biz20	Limestone	0.25	0.02	15
<i>Barre a Pecten Fm.</i>				
Biz1	Limestone	0.31	0.02	12

¹ Total organic carbon (wt.%). ² Insoluble residue (wt.%).

4.2. Optical Characteristics of Solid Bitumen

Solid bitumen dominated, almost entirely, the organic isolate, displaying an amorphous feature, dark brown color in transmitted white light, and no fluorescence (Figure 3A–I). Most of the particles presented a smooth surface, with the presence of fractures, a characteristic that permitted the separation between the solid bitumen and the amorphous organic matter (Figure 3A–I). Some of the solid bitumen particles displayed a cratered aspect that resulted from the dissolution of the mineral matter by the acid maceration treatment performed for kerogen isolation (Figure 3H). In addition to the solid bitumen, the isolated kerogen association showed the presence, in very small quantities, of phytoclasts, zooclasts and some palynomorphs (sporomorphs, dinoflagellate cysts, and undifferentiated palynomorphs). The sporomorphs present in the samples were used for the determination of SCI (Figure 3J–L). SEM analysis exhibited a plate-like form for the solid bitumen (Figure 4) with stratified borders (Figure 4F), sometimes with the presence of inclusions of phytoclasts or palynomorphs. The presence of fractures in the bitumen particles was frequent (Figure 4).

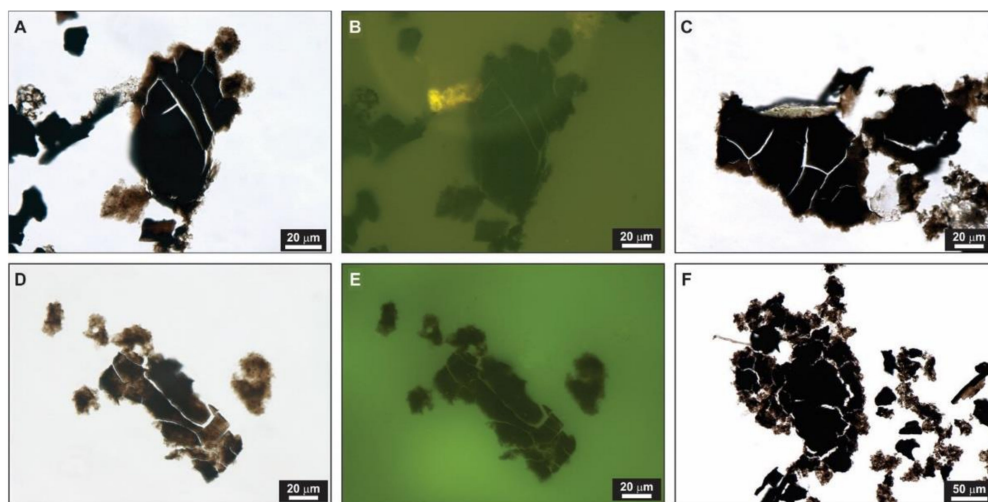


Figure 3. Cont.

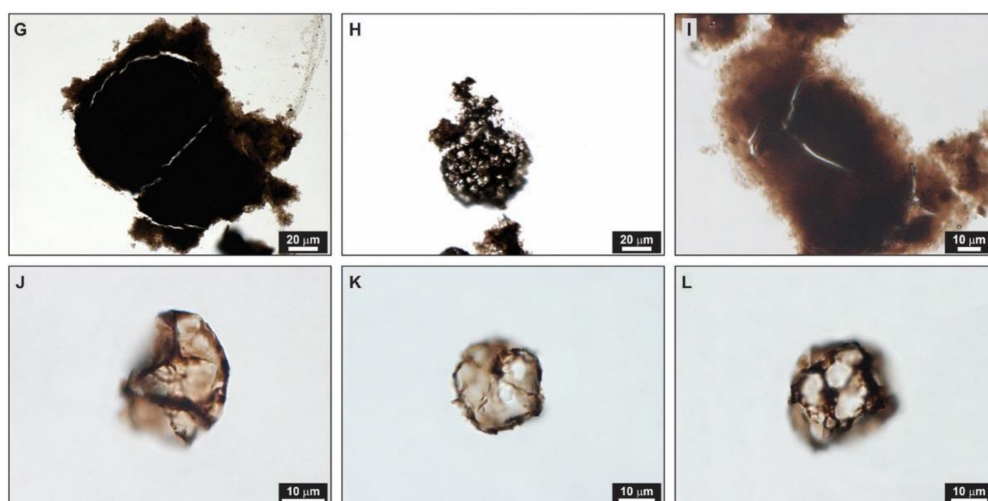


Figure 3. Photomicrographs of solid bitumen and spores in isolated kerogen slides. Transmitted white light (A,C,D,F–L); fluorescence mode (B,E).

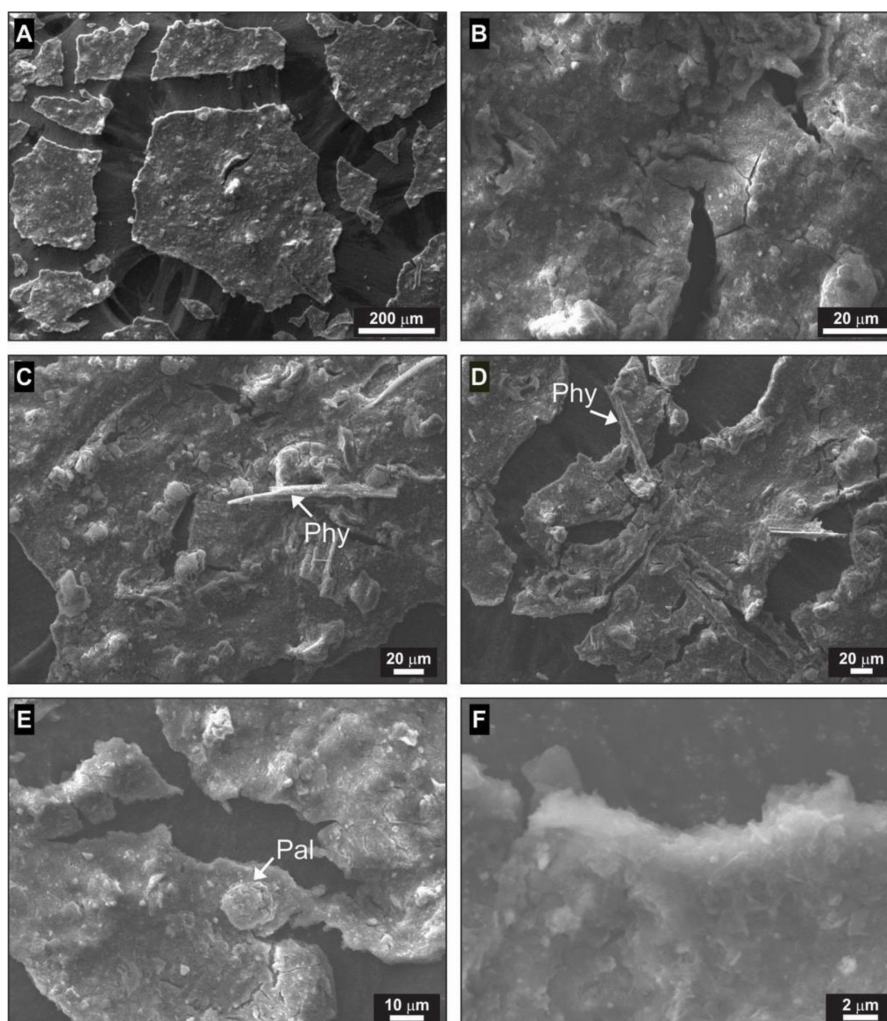


Figure 4. (A–F) Photomicrographs of solid bitumen taken by SEM. Phy: phytoclast; Pal: palynomorph.

Following the identification of the bitumen in the isolated kerogen, a petrographic analysis (using reflected white and incident blue lights) was performed to assess the organic

material's features and its spatial relation with the mineral matrix. Solid bitumen appears mostly filling voids, especially in carbonate particles, and fractures in the mineral matrix.

The petrographic analysis exposed differences in the optical characteristics of the solid bitumen concerning its reflectance, fluorescence, and texture. These differences allowed the identification of four groups of the solid bitumen that are described in detail below (Sections 4.3–4.6). The four families of the bitumen (A–D) present a very wide range of mean reflectance values, from 0.21% to 2.64% BR_r (Table 2). Based on the reflectance data and fluorescence features, solid bitumen A can be classified as glance pitch [14] or solid bitumen [15]; solid bitumen B and C—as epi-impsonite [14] or pyrobitumen [15]; solid bitumen D—as meso-impsonite [14] or pyrobitumen [15]. According to Mastalerz et al. [6], solid bitumen A and B is classified as solid bitumen, and solid bitumen C and D—as pyrobitumen.

Table 2. Mean random reflectance of solid bitumen.

Sample	Solid Bitumen A				Solid Bitumen B				Solid Bitumen C				Solid Bitumen D			
	%BR _r ¹	Stdev ²	n ³	%VR _{eq} ⁴	%BR _r ¹	Stdev ²	n ³	%VR _{eq} ⁴	%BR _r ¹	Stdev ²	n ³	%VR _{eq} ⁴	%BR _r ¹	Stdev ²	n ³	%VR _{eq} ⁴
	<i>Argilites noires litées Mb.</i>															
Biz125	0.32	0.06	31	0.60	0.94	0.08	56	0.98	1.47	0.27	9	1.31	2.52	0.21	9	1.96
Biz115	0.21	0.03	25	0.53	0.80	0.09	50	0.89	1.53	0.25	6	1.35	2.34	0.25	3	1.85
	<i>Schistes carton Mb.</i>															
Biz100	0.25	0.04	17	0.55	0.86	0.15	17	0.93	1.41	0.22	6	1.27	2.64	0.35	3	2.03
Biz80	0.30	0.11	16	0.59	0.74	0.14	50	0.86	1.48	0.26	7	1.31	2.09	–	1	1.69
Biz60	0.29	0.07	33	0.58	0.79	0.13	29	0.89	1.58	–	1	1.38	2.20	0.28	2	1.76
Biz40	0.29	0.06	30	0.58	0.70	0.13	14	0.83	1.17	0.08	2	1.12	–	–	–	–
Biz30	0.39	–	1	0.64	0.80	0.13	83	0.89	1.40	0.25	2	1.27	–	–	–	–
Biz20	0.30	0.10	5	0.59	0.93	0.12	11	0.97	1.58	0.24	48	1.38	2.15	0.11	6	1.73
	<i>Barre a Pecten Fm.</i>															
Biz1	0.38	0.02	2	0.63	0.94	0.12	9	0.98	1.58	0.25	38	1.38	2.38	0.34	14	1.87

Note: ¹ % BR_r: mean random reflectance (%); ² Stdev: standard deviation; ³ n: number of measurements; ⁴ % VR_{eq}: equivalent vitrinite reflectance (%) according to [14].

4.3. Solid Bitumen A

Solid bitumen A was observed in all the samples from the Bizanet section, but in lower amounts than solid bitumen B. It appeared with higher incidence in the samples from the Schistes carton Mb. and the Argilites noires litées Mb. (Biz40, Biz60, Biz80, Biz100, Biz115, and Biz125; Table 2). Under reflected white light, this solid bitumen displayed a dark color and a brittle aspect. Under incident blue light, the particles presented mostly a brown color, with some particles presenting areas with an orange fluorescence color. Solid bitumen A appeared mostly filling spaces or fractures in the mineral matrix, with the particle size reaching more than 1 mm. Most of the particles presented fractures (Figure 5). The shape of the solid bitumen differed according to the space where it occurred. The mean random reflectance varied from 0.21% to 0.39% BR_r (average, 0.30% BR_r; Table 2).

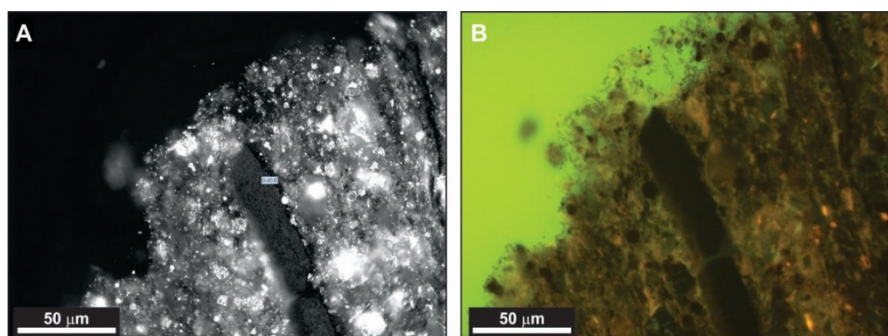


Figure 5. Cont.

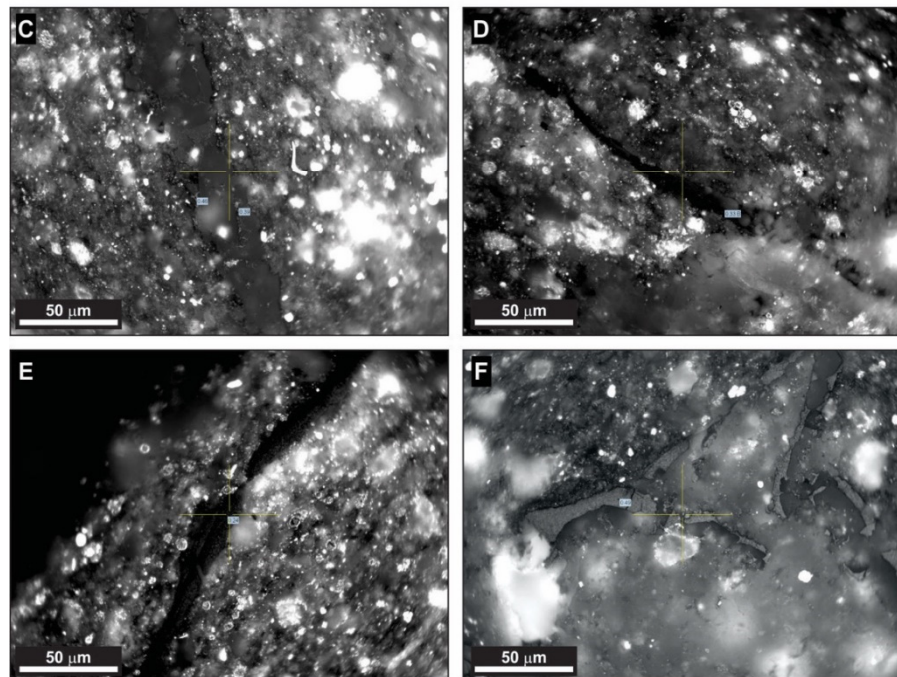


Figure 5. Photomicrographs of solid bitumen A in whole-rock polished blocks. Reflected white light (A,C–F); fluorescence mode (B).

4.4. Solid Bitumen B

Solid bitumen B was the most common of the solid bitumen families, appearing in all the studied samples in a higher quantity, especially in the samples from the Schistes carton Mb. And the Argilites noires litées Mb. (Biz30, Biz60, Biz80, Biz115, and Biz125; Table 2). This solid bitumen presented, under reflected white light, a grey color, and an irregular surface, was optically isotropic, and displayed no fluorescence under incident blue light. Solid bitumen B appeared mostly filling voids in the mineral matrix, usually associated with carbonate grains, with its shape varying according to the space where it occurred. Most of the particles presented fractures (Figure 6). Due to the prevalence of this solid bitumen, the presence of fractures within the particles, and the absence of fluorescence, this should correspond to most of the solid bitumen observed in the palynofacies slides under transmitted white light. The mean random reflectance ranged from 0.70% to 0.94% BR_r (average, 0.89% BR_r; Table 2).

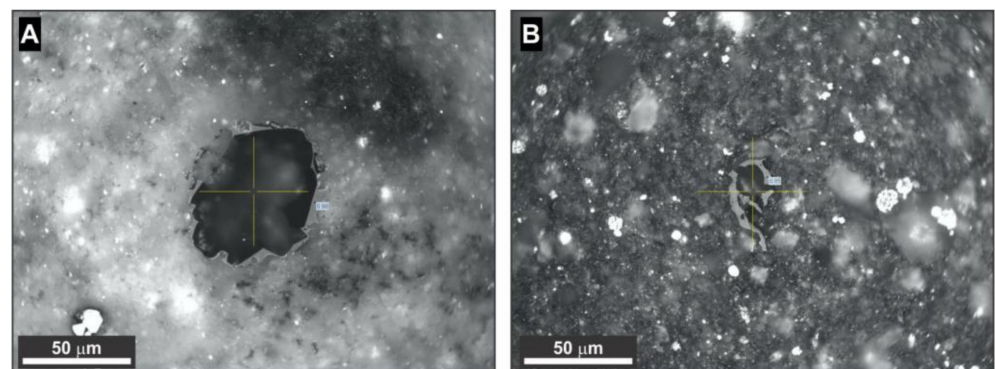


Figure 6. Cont.

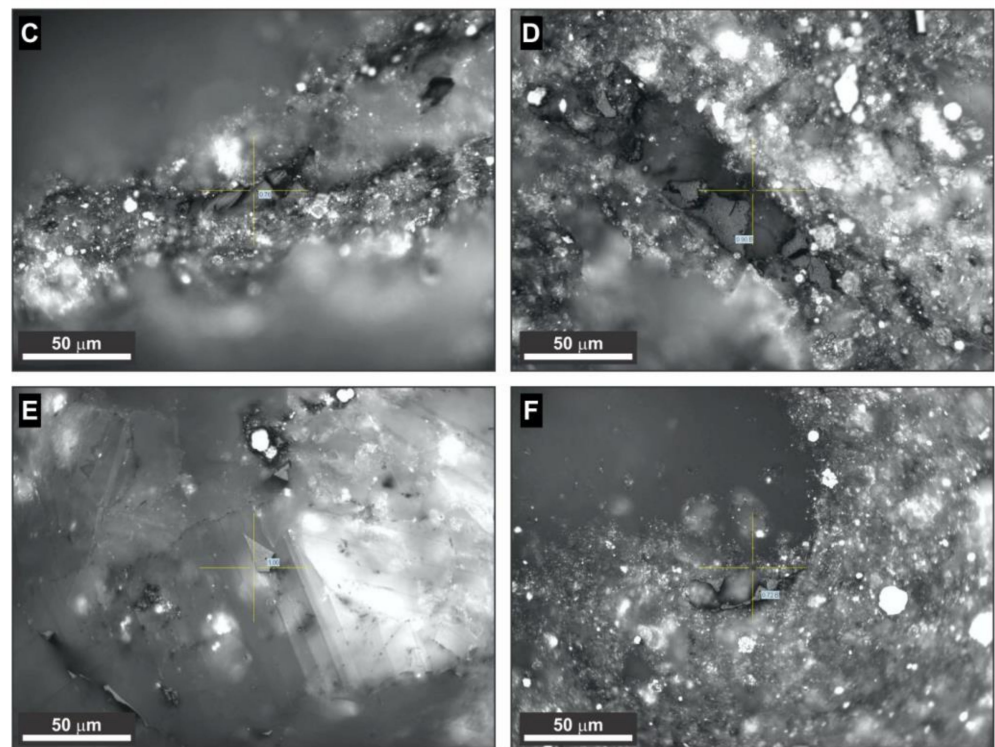


Figure 6. (A–F) Photomicrographs of solid bitumen B in whole-rock polished blocks under reflected white light.

4.5. Solid Bitumen C

Solid bitumen C was present in all the studied samples, with a higher incidence in the samples with lower IR (Biz1 and Biz20; Table 2). Under reflected white light, it displayed a grey color, a smooth surface, was optically isotropic, and displayed no fluorescence under incident blue light. This solid bitumen appears filling voids in the mineral matrix and is particularly associated with carbonate grains. Its shape varied according to the space where it occurred (Figure 7). The mean random reflectance ranged from 1.17% to 1.58% BR_r (average, 1.47% BR_r ; Table 2).

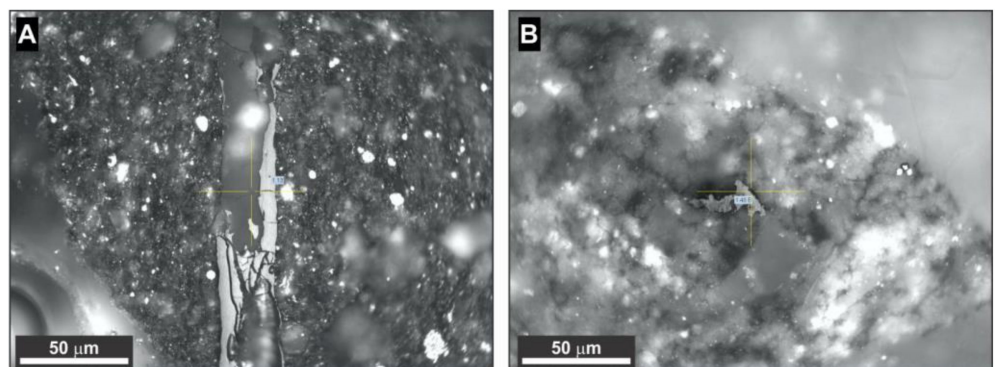


Figure 7. Cont.

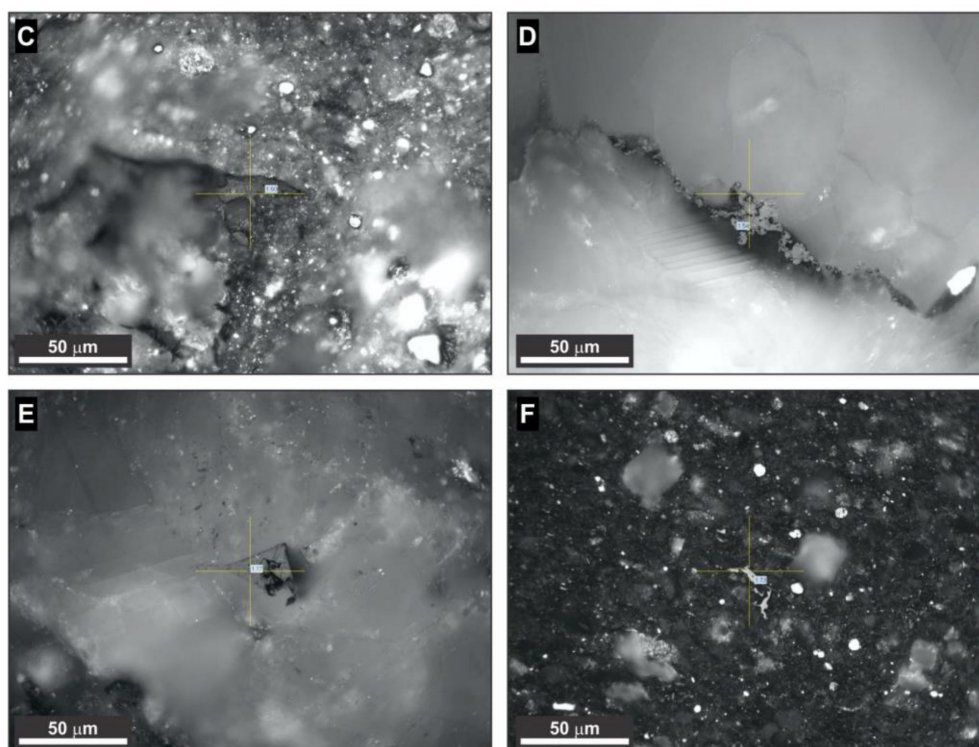


Figure 7. (A–F) Photomicrographs of solid bitumen C in whole-rock polished blocks under reflected white light.

4.6. Solid Bitumen D

Solid bitumen D was observed in small quantities in many of the samples from the Bizanet section, except for samples Biz20 and Biz40. It appeared with a lower incidence in the samples from the Schistes carton Mb. (Table 2). Under reflected white light, this solid bitumen displayed homogenous optical properties, a grey color, a smooth surface with high-quality polishing, and was isotropic. Under incident blue light, the particles presented no fluorescence. This solid bitumen appeared mostly filling voids in the mineral matrix, with a higher prevalence in carbonate grains, with the shape of the solid bitumen varying according to the space where it occurred (Figure 8). The mean random reflectance varied from 2.09% to 2.64% BR_r (average, 2.33% BR_r; Table 2).

4.7. Relationship between SCI and Solid Bitumen

Through the analysis of isolated kerogen using transmitted white light, SCI was determined in most of the samples, with values higher than 9–9.5. This corresponds to an equivalent vitrinite value (R_{eq}) of >1.50% according to the %R_r, SCI, temperature, and age correlation chart proposed by Fisher et al. [41] (Figure 3J–L). These values indicate that OM is in an overmature stage.

In the samples with various populations of solid bitumen, the non-migrated (indigenous) solid bitumen reflectance is the aspect used to correlate with vitrinite reflectance values and, therefore, to assess the thermal maturity of OM of the sample e.g., [6,14]. Comparing the equivalent vitrinite values of SCI and of the solid bitumen, only solid bitumen D showed equivalent vitrinite values inside the interval of the equivalent vitrinite of SCI, being therefore the only one that could be considered as a possibly indigenous bitumen (Figure 9; Table 2). No trend was observed in the VR_{eq} values of the different families of solid bitumen when plotted against depth (Figure 9). Nevertheless, it is probable that solid bitumen D is the indigenous population, while the other families of solid bitumen present in the samples must be migrated.

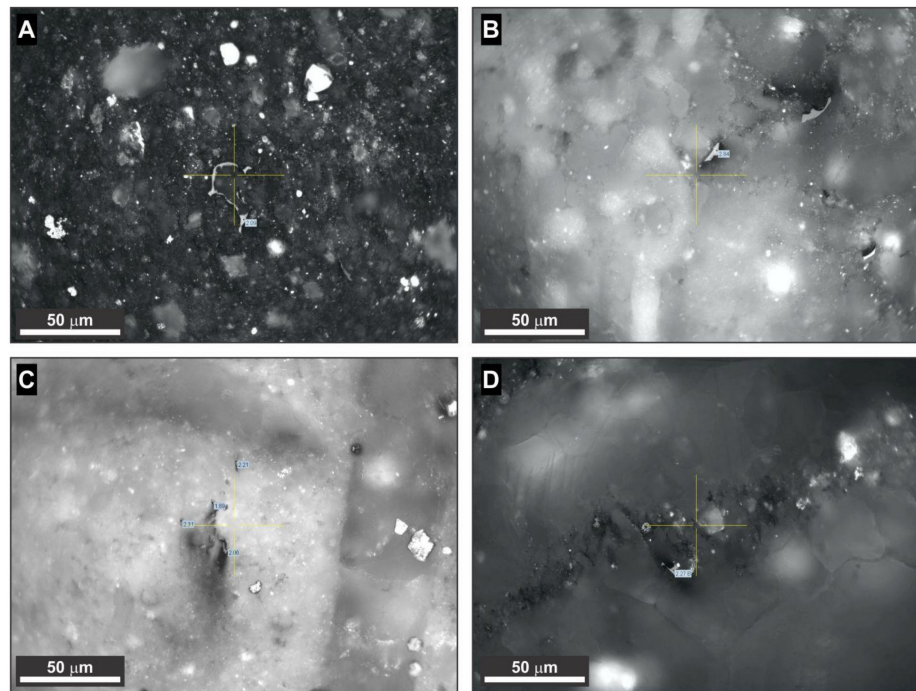


Figure 8. (A–D) Photomicrographs of solid bitumen D in whole-rock polished blocks under reflected white light.

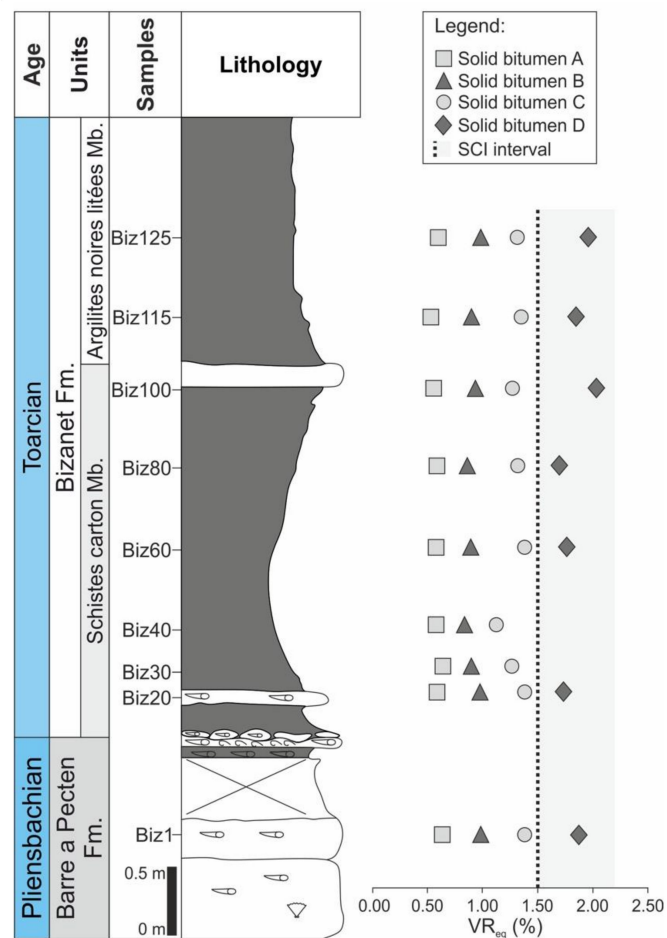


Figure 9. Vertical plot of the solid bitumen equivalent vitrinite reflectance (%) values of all the samples and the spore coloration index (SCI) interval.

4.8. Solid Bitumen Source

As discussed in Section 4.7, three of the four families of solid bitumen (A–C) identified in the Bizanet section are migrated (underwent migration processes, “migrabitumen” *sensus* Jacob [14]) and could possibly have been produced at hundreds of miles away from the reservoir. The identification of different populations of bitumen in the same rocks, identified here as solid bitumen A–D, could indicate the occurrence of several thermal events and/or pulses of hydrocarbons migration e.g., [6,13,23].

In a petrographic thermal maturity assessment study of the organic-rich sediments of the Pont de Suert section (in the same Pyrenean Basin), a lateral equivalent to the Bizanet section in the South Pyrenean Zone, Fonseca et al. [32] did not report the presence of any solid bitumen in the same stratigraphic interval. This could indicate that the presence of these components at Bizanet could be related to the differences in the morphotectonic contexts in which these sections are inserted. In fact, when analyzing the structural context around Bizanet, several pathways of migration can be identified, especially the presence of the North Pyrenean Thrust Fault, a major thrust very near the Bizanet section’s location (Figure 10).

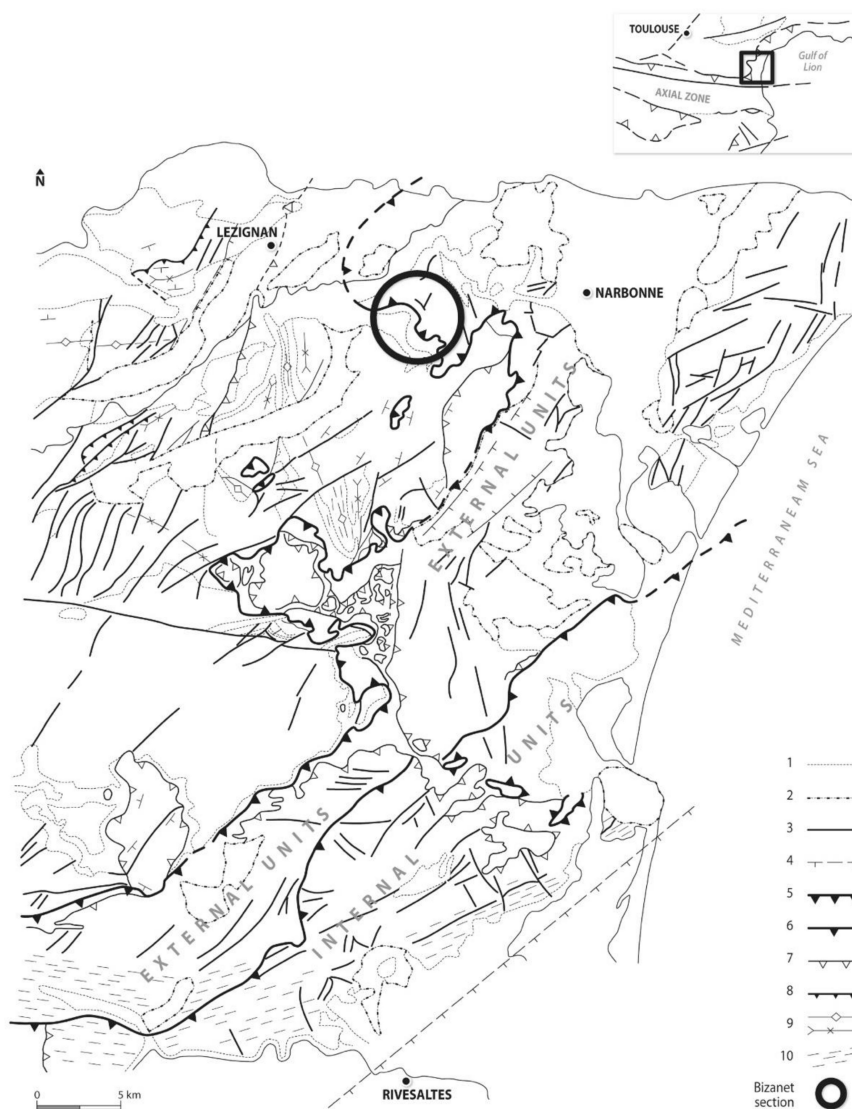


Figure 10. Simplified structural map of the Corbières nappe with the location of the Bizanet section (modified from Viallard [35]). 1: pre-Oligocene stratigraphic contact; 2: post-nappe terranes; 3: subvertical fault; 4: main normal fault; 5: basal contact in allochthonous units; 6: frontal thrusts in internal units; 7: tangential shear surface; 8: foreland thrusts; 9: folds axis; 10: cleavage.

5. Conclusions

Four families of solid bitumen (A–D) were identified in the late Pliensbachian–early Toarcian carbonate deposits from the Bizanet section (Pyrenean Basin) using optical microscopy techniques. These bitumen families differ in terms of their optical properties and present a large range of reflectance (glance pitch, epi- and meso-impsonite). The presence of spores in the same samples allowed the assessment of the OM thermal maturity using SCI and the comparison between the equivalent vitrinite values of SCI and of the different populations of solid bitumen. Solid bitumen D displays equivalent vitrinite values in accordance with the ones determined through SCI and is therefore considered an indigenous bitumen while the other three populations (A–C) are migrated. The absence of solid bitumen in a laterally equivalent section in the South Pyrenean Zone (Pont de Suert section) could indicate that the migration of these hydrocarbons could be influenced by the morphotectonic context of the Bizanet section, namely, the presence of a major thrust fault in the eastern Corbières close to the section’s location.

Author Contributions: Conceptualization, C.F., J.G.M.F., C.L., and L.V.D.; Formal analysis, C.F.; Investigation, C.F., C.L., and F.S.d.S.; Methodology, C.F. and J.G.M.F.; Project administration, C.F. and C.L.; Resources, J.G.M.F. and C.L.; Supervision, J.G.M.F., C.L., and L.V.D.; Validation, J.G.M.F. and C.L.; Visualization, C.F.; Writing—original draft preparation, C.F.; Writing—review and editing, J.G.M.F., C.L., and L.V.D. All authors have read and agreed to the published version of the manuscript.

Funding: This research received no external funding.

Data Availability Statement: The data presented in this study are available in the article.

Acknowledgments: The authors thank the team of the Laboratory of Palynofacies and Organic Facies of the Federal University of Rio de Janeiro (LAFO-UFRJ) for their technical support in sample preparation and all geochemical analyses and the Department of Geosciences, Environment, and Spatial Planning of the Faculty of Sciences of the University of Porto (DGAOT-FCUP), and the Institute of Earth Sciences (ICT) for allowing access to their Laboratory of Organic Petrography, where all petrographic analyses were performed.

Conflicts of Interest: The authors declare no conflict of interest.

References

1. Tissot, B.; Welte, D.H. *Petroleum Formation and Occurrence*, 2nd ed.; Springer: Berlin, Germany, 1984.
2. Jacob, H. Dispersed solid bitumens as an indicator for migration and maturity in prospecting for oil and gas. *Erdöl Und Kohle-Erdgas-Petrochem.* **1985**, *38*, 365.
3. Hunt, J.M. *Petroleum Geochemistry and Geology*, 2nd ed.; W.H. Freeman and Company: New York, NY, USA, 1996.
4. Jarvie, D.M.; Hill, R.J.; Ruble, T.E.; Pollastro, R.M. Unconventional shale-gas systems: The Mississippian Barnett shale of north-Central Texas as one model for thermogenic shale-gas assessment. *Am. Assoc. Pet. Geol. Bull.* **2007**, *91*, 475–499. [[CrossRef](#)]
5. Vandenbroucke, M.; Largeau, C. Kerogen origin, evolution and structure. *Org. Geochem.* **2007**, *38*, 719–833. [[CrossRef](#)]
6. Mastalerz, M.; Drobnik, A.; Stankiewicz, A.B. Origin, properties, and implications of solid bitumen in source-rock reservoirs: A review. *Int. J. Coal Geol.* **2018**, *195*, 14–36. [[CrossRef](#)]
7. Huc, A.Y.; Nederlof, P.; Debarre, R.; Carpentier, B.; Boussafir, M.; Laggoun-Defarge, F.; Lenail-Chouteau, A.; Bordas-Le Floch, N. Pyrobitumen occurrence and formation in a Cambro-Ordovician sandstone reservoir, Fahud salt basin, North Oman. *Chem. Geol.* **2000**, *168*, 9–112. [[CrossRef](#)]
8. Walters, C.C.; Kelemen, S.R.; Kwiatek, P.J.; Pottorf, R.J.; Mankiewicz, P.J.; Curry, D.J.; Putney, K. Reactive polar precipitation via ether cross-linkage: A new mechanism for solid bitumen formation. *Org. Geochem.* **2006**, *37*, 408–427. [[CrossRef](#)]
9. Rippen, D.; Littke, R.; Bruns, B.; Mahlstedt, N. Organic geochemistry and petrography of Lower Cretaceous Wealden black shales of the Lower Saxony Basin: The transition from lacustrine oil shales to gas shales. *Org. Geochem.* **2013**, *63*, 18–36. [[CrossRef](#)]
10. Kondla, D.; Sanei, H.; Embry, A.; Ardakani, O.H.; Clarkson, C.R. Depositional environment and hydrocarbon potential of the middle Triassic strata of the Sverdrup Basin, Canada. *Int. J. Coal Geol.* **2015**, *147–148*, 71–84. [[CrossRef](#)]
11. Emmanuel, S.; Eliyahu, M.; Day-Stirrat, R.J.; Hofmann, R. Impact of thermal maturation on nano-scale elastic properties of organic matter in shales. *Mar. Pet. Geol.* **2016**, *70*, 175–184. [[CrossRef](#)]
12. Hackley, P.C.; Cardott, B.J. Application of organic petrography in North America shale petroleum systems: A review. *Int. J. Coal Geol.* **2016**, *163*, 8–51. [[CrossRef](#)]

13. Gentzis, T.; Goodarzi, F. A review of the use of bitumen reflectance in hydrocarbon exploration with examples from Melville Island, Arctic Canada. In *Applications of Thermal Maturity Studies to Energy Exploration*; Nuccio, V.F., Barker, C.E., Eds.; SEPM: Broken Arrow, OK, USA, 1990; pp. 23–36.
14. Jacob, H. Classification, structure, genesis and practical importance of natural solid oil bitumen (“migrabitumen”). *Int. J. Coal Geol.* **1989**, *11*, 65–79. [[CrossRef](#)]
15. Landis, C.R.; Castañó, J.R. Maturation and bulk chemical properties of a suite of solid hydrocarbons. *Org. Geochem.* **1995**, *22*, 137–149. [[CrossRef](#)]
16. Curiale, J.A. Origin of solid bitumens, with emphasis on biological marker results. *Org. Geochem.* **1986**, *10*, 559–580. [[CrossRef](#)]
17. Curiale, J.A.; Harrison, W.E.; Smith, G. Sterane distribution of solid bitumen pyrolyzates. Changes with biodegradation of crude oil in Ouachita Mountains, Oklahoma. *Geochim. Cosmochim. Acta* **1983**, *47*, 517–523. [[CrossRef](#)]
18. Bertrand, R.; Héroux, Y. Chitinozoan, graptolite and scolecodont reflectance as an alternative to vitrinite and pyrobitumen reflectance in Ordovician and Silurian Strata, Anticosti Island, Quebec, Canada. *Am. Assoc. Pet. Geol. Bull.* **1987**, *71*, 951–957.
19. Bertrand, R. Correlations among the reflectances of vitrinite, chitinozoans, graptolites and scolecodonts. *Org. Geochem.* **1990**, *15*, 565–574. [[CrossRef](#)]
20. Bertrand, R. Standardization of solid bitumen reflectance to vitrinite in some Paleozoic sequences of Canada. *Energy Sources* **1993**, *15*, 269–287. [[CrossRef](#)]
21. Fowler, M.G.; Kirste, D.M.; Goodarzi, F.; Macqueen, R.W. Optical and geochemical classification of Pine Point bitumens and evidence for their origin from two separate source rocks. *Energy Sources* **1993**, *15*, 315–337. [[CrossRef](#)]
22. Riediger, C.L. Solid bitumen reflectance and Rock-Eval Tmax as maturation indices: An example from the “Nordegg Member”, Western Canada Sedimentary Basin. *Int. J. Coal Geol.* **1993**, *22*, 295–315. [[CrossRef](#)]
23. Stasiuk, L.D. The origin of pyrobitumens in Upper Devonian Leduc Formation gas reservoirs, Alberta, Canada: An optical and EDS study of oil to gas transformation. *Mar. Pet. Geol.* **1997**, *14*, 915–929. [[CrossRef](#)]
24. Hwang, R.J.; Teerman, S.C.; Carlson, R.M. Geochemical comparison of reservoir solid bitumens with diverse origins. *Org. Geochem.* **1998**, *29*, 505–517. [[CrossRef](#)]
25. George, S.C.; Volk, H.; Ahmed, M.; Pickel, W.; Allan, T. Biomarker evidence for two sources for solid bitumens in the Subu wells: Implications for the petroleum prospectivity of the East Papuan Basin. *Org. Geochem.* **2007**, *38*, 609–642. [[CrossRef](#)]
26. Schoenherr, J.; Littke, R.; Urai, J.L.; Kukla, P.A.; Rawahi, Z. Polyphase thermal evolution in the infra-Cambrian Ara Group (South Oman Salt Basin) as deduced by maturity of solid reservoir bitumen. *Org. Geochem.* **2007**, *38*, 1293–1318. [[CrossRef](#)]
27. Kelemen, S.R.; Walters, C.C.; Kwiatek, P.J.; Afeworki, M.; Sansone, M.; Freund, H.; Pottorf, R.J.; Machel, H.G.; Zhang, T.; Ellis, G.S.; et al. Distinguishing solid bitumens formed by thermochemical sulfate reduction and thermal chemical alteration. *Org. Geochem.* **2008**, *39*, 1137–1143. [[CrossRef](#)]
28. Kelemen, S.R.; Walters, C.C.; Kwiatek, P.J.; Freund, H.; Afeworki, M.; Sansone, M.; Lamberti, W.A.; Pottorf, R.J.; Machel, H.G.; Peters, K.E.; et al. Characterization of solid bitumens originating from thermal chemical alteration and thermo-chemical sulfate reduction. *Geochim. Cosmochim. Acta* **2010**, *74*, 5305–5332. [[CrossRef](#)]
29. Shalaby, M.R.; Hakimi, M.H.; Abdullah, W.H. Geochemical characterization of solid bitumen (migrabitumen) in the Jurassic sandstone reservoir of the tut field, Shushan Basin, northern Western Desert of Egypt. *Int. J. Coal Geol.* **2012**, *100*, 26–39. [[CrossRef](#)]
30. Gonçalves, P.A.; Mendonça Filho, J.G.; Silva, F.S.; Flores, D. Solid bitumen occurrences in the Arruda sub-basin (Lusitanian Basin, Portugal): Petrographic features. *Int. J. Coal Geol.* **2014**, *139*, 217–227. [[CrossRef](#)]
31. Sanei, H. Genesis of solid bitumen. *Sci. Rep.* **2020**, *10*, 15595. [[CrossRef](#)]
32. Fonseca, C.; Mendonça, J.O.; Mendonça Filho, J.G.; Lézin, C.; Duarte, L.V. Thermal maturity assessment study of the late Pliensbachian-early Toarcian organic-rich sediments in Southern France: Grands Causses, Quercy and Pyrenean basins. *Mar. Pet. Geol.* **2018**, *91*, 338–349. [[CrossRef](#)]
33. Fauré, P. Le lias des Pyrénées. *Strata* **2002**, *2*, 761.
34. Boix, C.; Perez, R. The position of the south pyrenean margin in the late cretaceous: Evidence for larger foraminifera. In Proceedings of the AAPG International Conference, Barcelona, Spain, 21–24 September 2003.
35. Viillard, P. Un modèle de charriage épiglyptique: La nappe des Corbières orientales (Aude, France). *Bull. Soc. Géol. Fr.* **1987**, *III*, 551–559. [[CrossRef](#)]
36. ASTM. *Standard Test Methods for Sulfur in the Analysis Sample of Coal and Coke Using High-Temperature Tube Furnace Combustion Methods*; ASTM International: West Conshohocken, PA, USA, 2008.
37. United States Environmental Protection Agency (USEPA). *Methods for the Determination of Total Organic Carbon (TOC) in Soils and Sediments*; Office of Research and Development: Las Vegas, NV, USA, 2002.
38. Mendonça Filho, J.G.; Menezes, T.R.; Mendonça, J.O.; Oliveira, A.D.; Silva, T.F.; Rondon, N.F.; Silva, F.S. Organic facies: Palynofacies and organic geochemistry approaches. In *Geochemistry—Earth’s System Processes*; Panagiotaras, D., Ed.; InTech: Rijeka, Croatia, 2012; pp. 211–248.
39. Mendonça Filho, J.G.; Menezes, T.R.; Mendonça, J.O. Organic composition (palynofacies analysis). In *7th ICCP Training Course on Dispersed Organic Matter*; GFZ: Potsdam, Germany, 2014; pp. 36–89.
40. Tyson, R.V. *Sedimentary Organic Matter. Organic Facies and Palynofacies*; Chapman and Hall: London, UK, 1995.

41. Fisher, M.J.; Barnard, P.C.; Cooper, B.S. Organic maturation and hydrocarbon generation in the mesozoic sediments of the sverdrup basin, arctic Canada. In Proceedings of the IV International Palynological Conference, Lucknow, India, 29 December 1976–15 January 1977; pp. 581–588.
42. ISO. *Methods for the Petrographic Analysis of Coals—Part 2: Methods of Preparing Coal Samples*; ISO: Geneva, Switzerland, 2009.
43. ASTM. *Standard Test Method for Microscopical Determination of Reflectance of Vitrinite Dispersed in Sedimentary Rocks*; ASTM International: West Conshohocken, PA, USA, 2014.